Hindawi
Mathematical Problems in Engineering
Volume 2019, Article ID 8469868, 11 pages
https://doi.org/10.1155/2019/8469868

Research Article

Internal Combustion Engine Fault Identification Based on FBG Vibration Sensor and Support Vector Machines Algorithm

Faye Zhang[1], **Mingshun Jiang**[1], **Lei Zhang**[1], **Shaobo Ji**[2], **Qingmei Sui**[1], **Chenhui Su**[1], **and Shanshan Lv**[1]

[1]*School of Control Science and Engineering, Shandong University, Jinan 250061, China*
[2]*School of Mechanical Engineering, Shandong University, Jinan 250061, China*

Correspondence should be addressed to Faye Zhang; zhangfaye@sdu.edu.cn and Qingmei Sui; sdusuiqingmei@163.com

Received 21 February 2019; Accepted 16 April 2019; Published 16 May 2019

Academic Editor: Gabriele Cazzulani

State monitoring and fault diagnosis of an internal combustion engine are critical for complex machinery safety. In the present study, a high-frequency vibration system was proposed based on Fiber Bragg Grating (FBG) cantilever sensor and intelligent algorithm. Structural vibration signal containing fault information of engine valves and oil nozzle was identified by FBG sensors and preprocessed using wavelet decomposition and reconstruction. Moreover, vibration energy was taken as fault characteristics. Subsequently, a fault identification model was built based on multiclass v-support vector classification (v-SVC). Experimental tests on the valve fault and fuel injection advance angle fault were performed and presented to verify the efficacy of the proposed approach. The results here reveal that the proposed method exhibits excellent fault detection performance for ICE fault identification. Furthermore, the proposed method can achieve higher performance than other methods in the fault identification accuracy.

1. Introduction

The working state of valve or oil nozzle is an important condition for engines, covering all petrol engines and diesel engines. Any defect in valves or oil nozzle will lead to the loss of engine power and even cause permanent damage. Thus, to avoid fatal failure of valves or oil nozzle and to reduce the secondary damage caused by breakdowns, it is urgently required to detect valve or oil nozzle defects quickly and accurately [1, 2].

Vibration analysis is one of the techniques that have been used for engine condition monitoring and fault diagnosis successfully. While engine is operating with different faults, the corresponding vibration signal will change, as reflected in the resonant frequency component changes [3, 4]. With the advancement of fiber optic sensing technology, a novel principle and method has been provided for condition monitoring and diagnosis of machinery. FBG sensors exhibit compact structure, good insulation, easy installation, high reliability, easy to build sensor networks, and other prominent advantages [5, 6]. Accordingly, FBG sensors are considered an ideal choice for detecting engine vibration [7–9].

With the improvement in the precision of the engine, automatic intelligent diagnosis technology with accurate recognition and prediction results is urgently required. Thus far, numerous studies have been conducted on fault diagnosis algorithms, e.g., expert systems [10–12], artificial neural networks (ANN) [13–15], and fuzzy logic [16–18]. Expert system refers to the use of computer storage of human knowledge, which imitates the reasoning of solving a particular problem by human expert. ANN requires a huge amount of learning to build a fault model, which is employed to perform fault diagnosis. Fuzzy logic requires considerable system input and output signal characteristics to build a model of the membership function of various variables. However, these methods need many samples for training, thereby limiting the popularization and the application of

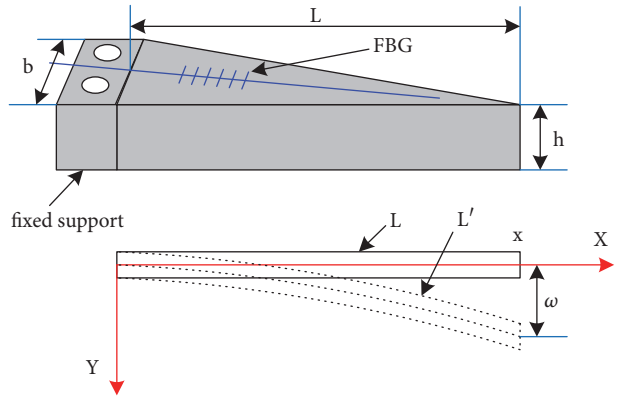

Figure 1: The architecture of FBG high-frequency vibration sensor.

the algorithm. Support vector machine (SVM) [19] is preferred for fault diagnosis for its high accuracy and good generalization even with small samples. Thus, the algorithm has been an effective method for diagnosing mechanical faults, e.g., bearing [20], gearbox [21], and centrifugal pump [22].

In this study, a high-frequency system was presented based on Fiber Bragg Grating (FBG) cantilever sensor and edge filter demodulation scheme to collect vibration signals of engine valves and oil nozzle. The signals were subsequently preprocessed by wavelet decomposition and reconstruction, and vibration energy was proposed to extract fault features. Next, a multifault diagnosis model based on v-SVC was built and verified on an internal combustion engine (ICE) by valve and fuel injection advance angle fault identification. The results reveal that the proposed method can achieve high predictive accuracy than the SOM neural network-based method, which was up to 95%.

2. Description of Proposed Algorithm

2.1. FBG High-Frequency Vibration Sensor Design. The sensor structure is shown in Figure 1. The sensor is composed of three parts, namely, an equi-intensity cantilever beam of dimensions $L \times b \times h$, a fixed support, and an FBG adhered on the cantilever.

Given the centroid of the equi-intensity cantilever beam with no-load locating at position $L/3$, the eigenfrequency is expressed as

$$f = \frac{1}{2\pi}\sqrt{\frac{k}{m}} = \frac{1}{2\pi}\sqrt{\frac{mg}{\omega \bullet \frac{L}{3}} \bullet \frac{1}{m}} = \frac{1}{2\pi}\sqrt{\frac{486Eh^2}{43\rho L^4}}. \quad (1)$$

The parameters of the sensor were set as listed in Table 1. The natural frequency is 14.8kHz, which is given by (1).

A finite element model of the first order was built to explore the harmonic response frequency characteristics of the sensor by ANSYS (Figure 2). The natural frequency is 8.9kHz, lower than the theoretical value caused by lateral vibration of the beam end. Besides, to the best of our knowledge, the papers on FBG vibration sensor with higher natural frequency have been rarely published.

Table 1: The parameters of FBG vibration sensor.

number	parameters	value
1	E	195GPa
2	ρ	8000kg/m^3
3	h	3.5 mm
4	L	25.0 mm
5	b	5.0 mm

2.2. FBG Demodulation System. The structure diagram of the demodulation system is given in Figure 3. The system consists of an ASE light source without flat processing, a circulator, a photoelectric conversion and amplification circuit, an FBG vibration sensor, and a data processing unit as well as a computer. The ASE light source offers the system a light source, and its spectral linear segment serves as an edge filter. The circulator provides an optical signal loop, while its unidirectional feature can prevent the transmission of the reflected light into the light source. The FBG vibration sensor converts the valve vibration signal into a light intensity signal. The intensity signal, which is collected by the data processing unit, is converted into a voltage signal by the photoelectric conversion circuit. The computer displays the voltage signal. The demodulation system works as follows: when reflection peak of FBG vibration sensors shifts $\Delta\lambda$, caused by engine structure failure vibration signals, its intensity will vary owing to the modulation effect of ASE source hypotenuse filter. This change is converted to a voltage signal by photoelectric conversion and amplification circuit. Afterwards, the voltage will be collected by the data processing unit and displayed by computer.

The peak sample frequency of the system is 200 kHz, and its demodulation precision is 2.5mV/pm. The wavelength of FBG sensor was set ranging from 1533 nm to 1536 nm, which is the maximum slope position of the ASE light source

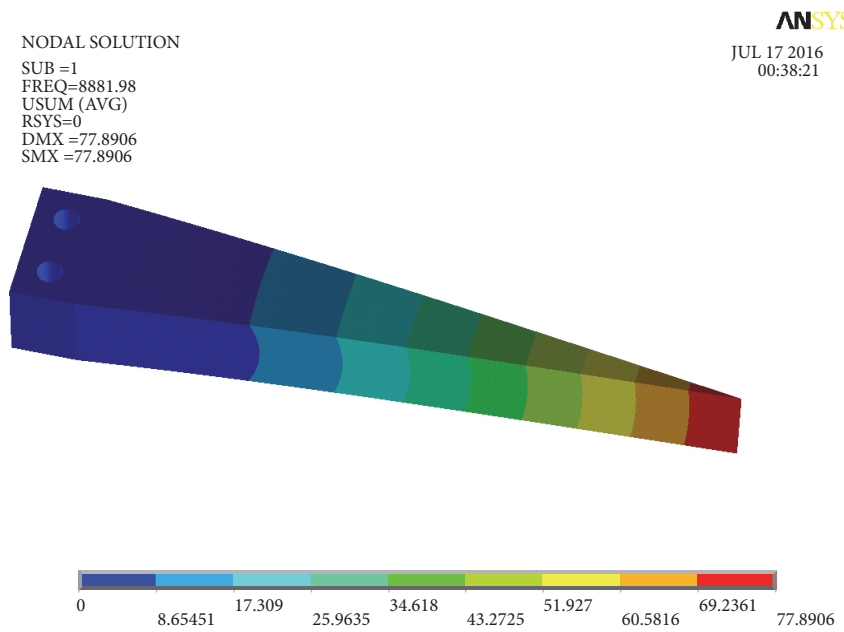

Figure 2: The finite element model.

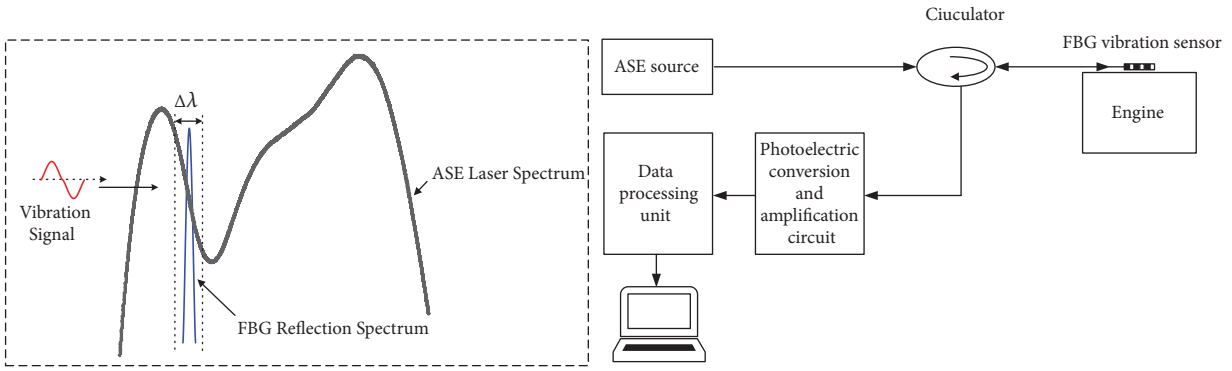

Figure 3: The structure diagram of FBG demodulation system.

spectral curve. Given the intensity of vibration signals, the wavelength was selected to be 1534 nm and stretched to 1534.570 nm by preloading.

2.3. Fault Diagnosis Formulation. The process of building the model, based on v-support vector classification (v-SVC) technology [23], is illustrated as follows.

To diagnose the fault, the convex optimization problem solved by v-SVC is defined as

$$\begin{aligned} \min_{\boldsymbol{w},b,\boldsymbol{\xi},\rho} \quad & \frac{1}{2}\boldsymbol{w}^T\boldsymbol{w} - v\rho + \frac{1}{l}\sum_{i=1}^{l}\xi_i \\ s.t. \quad & y_i\left(\left\langle \boldsymbol{w} \bullet \phi\left(\boldsymbol{x}_i\right)\right\rangle + b\right) \geq \rho - \xi_i \\ & \xi_i \geq 0,\ i = 1,\ldots,l,\ \rho \geq 0. \end{aligned} \tag{2}$$

l denotes the training sample count; $\boldsymbol{x}_i \in \boldsymbol{R}^n$, $i = 1, \ldots, l$ is the extracted fault features; n is feature dimension. $y_i \in \{1, -1\}$ is category label. $\boldsymbol{w}$ is normal vector; ξ_i is slack variable; $0 < v \leq 1$ is a hyperparameter that denotes an upper bound on the fraction of training errors and a lower bound of the fraction of support vectors; ϕ refers to a nonlinear function that maps the input space into a higher dimensional space, and ρ is threshold. The solution of (2) is obtained by its dual Lagrange equation

$$\begin{aligned} \max_{\alpha} \quad & T\left(\boldsymbol{\alpha}\right) = -\frac{1}{2}\sum_{i=1}^{l}\sum_{j=1}^{l} y_i y_j \alpha_i \alpha_j \left(\phi\left(\boldsymbol{x}_i\right), \phi\left(\boldsymbol{x}_j\right)\right) \\ s.t. \quad & \sum_{i=1}^{N} \alpha_i y_i = 0 \\ & 0 \leq \alpha_i \leq \frac{1}{N} \\ & \sum_{i=1}^{N} \alpha_i \geq v. \end{aligned} \tag{3}$$

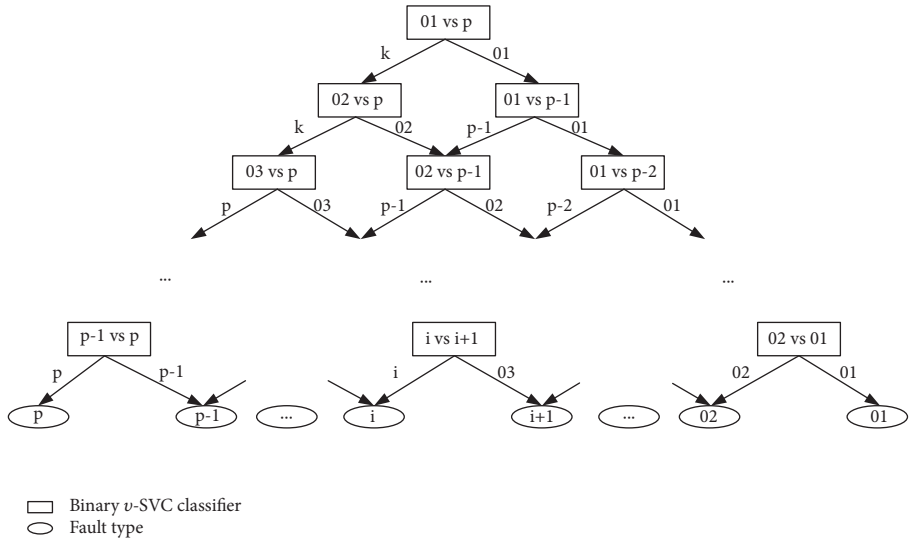

Figure 4: The fault type identification model.

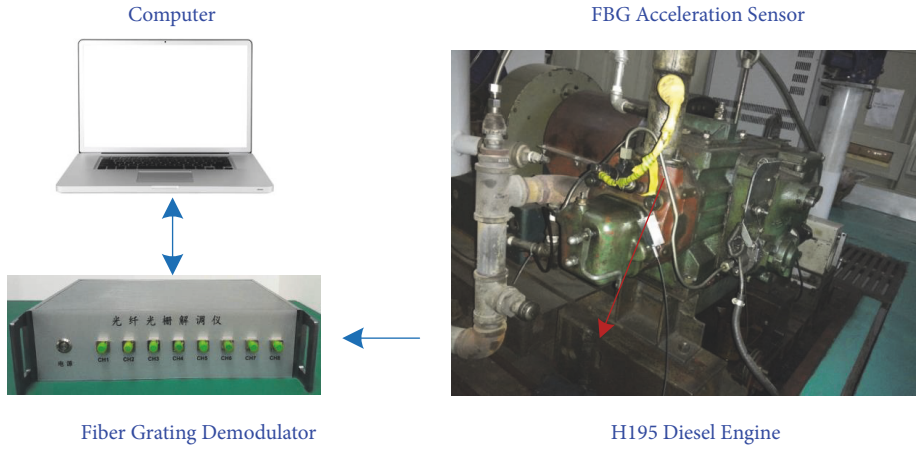

Figure 5: The engine vibration testing system.

$\boldsymbol{\alpha} = (\alpha_1, \alpha_2, \ldots, \alpha_N)$ refer to Lagrange multipliers. $k(\boldsymbol{x}_i, \boldsymbol{y}_j) = (\phi(\boldsymbol{x}_i), \phi(\boldsymbol{y}_j))$ is kernel function, which is taken as

$$k\left(\boldsymbol{x}_i, \boldsymbol{x}_j\right) = \exp^{-\gamma\|\boldsymbol{x}_i - \boldsymbol{x}_j\|}, \tag{4}$$

where γ denotes the nuclear wide. By solving (3) with (4), the final υ-SVC model can be expressed as

$$\begin{aligned} f(\boldsymbol{x}) &= \operatorname{sgn}\left(\sum_{i=1}^{l} \alpha_i y_i k\left(\boldsymbol{x}_i, \boldsymbol{x}\right) + b\right) \\ &= \operatorname{sgn}\left(\sum_{i=1}^{l} \alpha_i y_i \exp^{-\gamma\|\boldsymbol{x}_i - \boldsymbol{x}\|} + b\right). \end{aligned} \tag{5}$$

Equation (5) is the υ-SVC classifier model. If $f(\boldsymbol{x}) \geq 0$, the fault state belongs to fault type i and if $f(\boldsymbol{x}) < 0$. Thus, it does not belong to fault type i.

To solve multiclassification problems, multiclassifier based on directed acyclic graph (DAG) [24] and υ-SVC was proposed. Considering an example of p fault type, a total of $p(p+1)/2$ υ-SVC classifiers were built, and the fault diagnosis model based on υ-SVC and DAG is shown in Figure 4. The fault diagnosing process is as follows: when identifying any of the fault samples, first, start from 01 vs p; if the recognition result is fault 1, enter the right to 01 vs $p - 1$; otherwise, enter the left to 02 vs p. Repeat the mentioned process until arriving one node of the last layers of the model, which is the fault to be identified.

3. Experiments and Analysis

To validate the proposed fault diagnosis method, the valve and fuel injection advance angle fault experiment were performed.

3.1. Experiment Setup. The experimental setup used for valve fault diagnosis is shown in Figure 5. The test system consists of a H195 diesel engine, an FBG acceleration

Table 2: Experimental conditions set of valve experiment.

fault type	intake gap (mm)	outlet gap (mm)	load rate (%)	engine speed (rpm)	number of experiments
I	0.3	0.5	0	800	9
				1000	9
				1200	9
II	0.3	0.7	0	800	9
				1000	9
				1200	9
III	0.3	0.9	0	800	9
				1000	9
				1200	9
IV(normal state)	0.3	0.4	0	800	9
				1000	9
				1200	9
V	0.5	0.4	0	800	9
				1000	9
				1200	9
VI	0.7	0.4	0	800	9
				1000	9
				1200	9

Table 3: Experimental conditions set of fuel injection advance angle experiment.

fault type	Fuel injection advance angle (°)	load rate (%)	engine speed (rpm)	number of experiments
VII	16	0	800	9
			1000	9
			1200	9
VIII(normal state)	20	0	800	9
			1000	9
			1200	9
IX	24	0	800	9
			1000	9
			1200	9

sensor, and a fiber grating demodulator as well as a computer. The FBG acceleration sensor attached on cylinder head by epoxy adhesive sensed the vibration changes of engine structure and converted them into FBG wavelength changes. The wavelength changes were captured by the fiber grating demodulator and then transferred to computer via network.

In this case, nine types of fault types under no-load condition (e.g., normal state), shown in Tables 2 and 3, were involved in the experiment. The vibration signals were continuously acquired by the FBG vibration sensor, while keeping engine speed varied from 800 rpm to 1200 rpm at 200 rpm steps per min. 243 samples for fault type were acquired in the tests, while the sampling point was set to 40000. The waveforms of the nine operating states at 1200rmp in time domain are shown in Figure 6.

Figure 6 suggests that the dynamic signals were accurately detected by FBG acceleration sensor, which reveals that FBG sensor can be used for engine structural fault identification. However, the figure also suggests that it was hard to distinguish their fault state depending on the time domain vibration signals individually.

To find the differences between different fault types, the vibration signals collected at different valve clearance in time domain and frequency domain were analyzed. Normal state with valve clearance 0.4mm, intake valve clearance 0.3mm (s.t fault type IV), and abnormal state with intake valve clearance 0.7mm (s.t fault type VI) were taken as an example. The results are shown in Figure 7, showing that there were significant differences in frequency domain at 900 Hz~1400Hz and 1650 Hz~1850Hz.

3.2. Feature Extraction. To extract fault characteristics, the collected signals were decomposed by wavelet decomposition and reconstruction. Besides, the vibration energy was

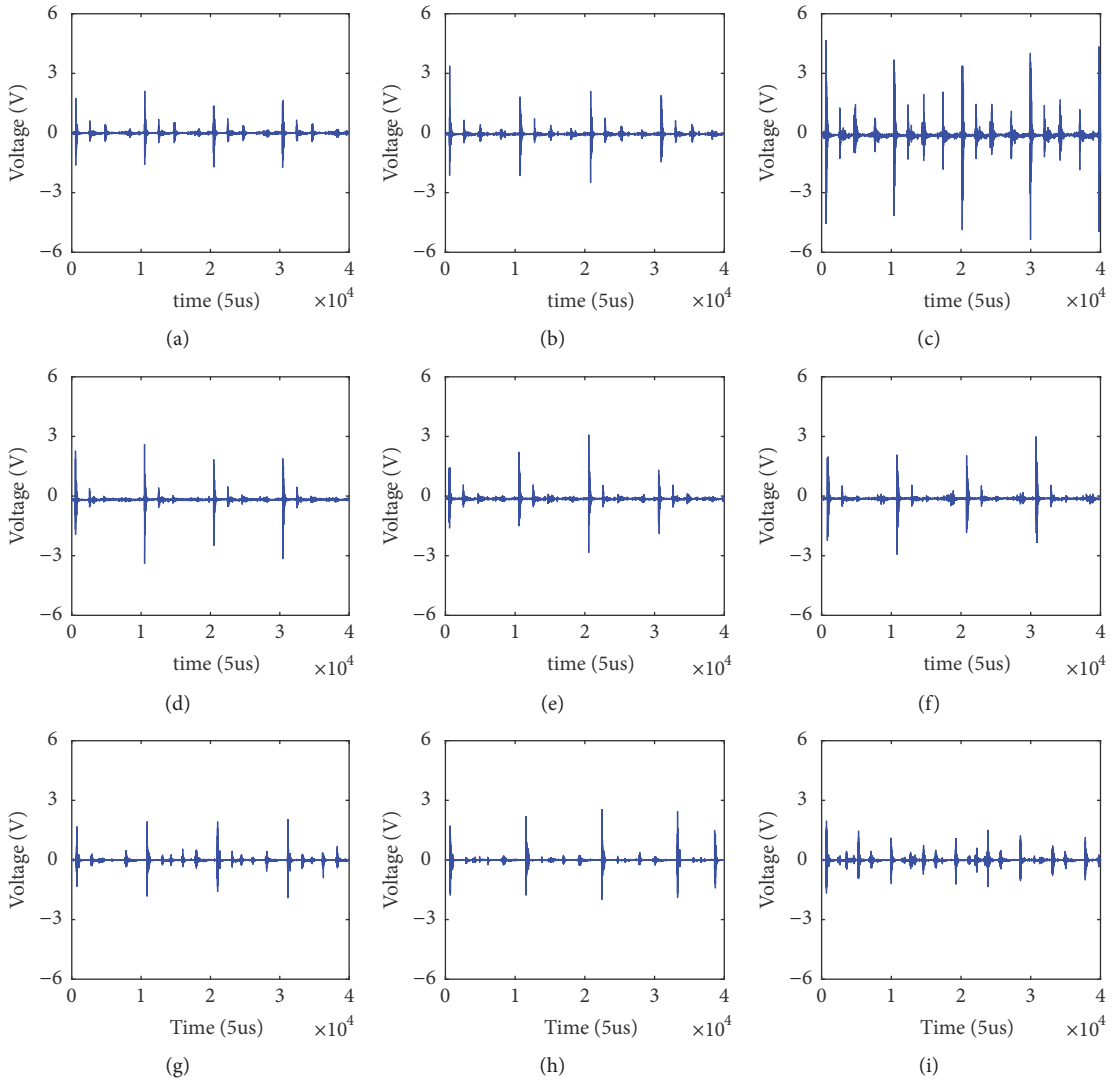

Figure 6: Time domain waveforms of the nine operating states: (a) fault type I, (b) fault type II, (c) fault type III, (d) fault type IV (normal state), (e) fault type V, (f) fault type VI, (g) fault type VII, (h) fault type VIII, and (i) fault type IX.

calculated by the processed formula, which was defined as follows.

Continuous vibration signals are denoted as function $f(t)$, which meet the following conditions within the range of real numbers:

$$\int_{-\infty}^{+\infty} \left|f\left(x\right)\right|^2 dx < +\infty. \tag{6}$$

Given the time series $F = (f(T), f(2T), \ldots, f(nT))$ obtained by sampling, the vibration energy is expressed as

$$E = \frac{1}{2\left(N_2 - N_1\right)} \sum_{i=N_1}^{N_2} \left|f\left(iT\right) - f\left(T_0\right)\right|^2. \tag{7}$$

$N_1 = 0, 1, 2, \ldots, n$, $N_2 = 1, 2, \ldots, n$, and $N_2 \geq N_1$. T denotes the sample Interval; n is the total sampling points. $f(T_0)$ is the initial state of the vibration signal.

The vibration signal of fault type I at 1000 rpm processed by wavelet decomposition and reconstruction with DB4 wavelet function is shown in Figure 8. Subsequently, the vibration energy of processed signals is calculated by (5). Three samples of each fault type were taken as examples. The results, used as feature vectors, are listed in Table 4.

To conclude the relationship between the vibration energy and the engine fault directly, the first feature vector of each fault type was normalized and plotted in the same coordinate system, as shown in Figure 9.

Figure 9 shows that all faults have different feature vectors. Accordingly, the vibration energy of decomposed vibration signals can be extracted as the fault characteristic.

3.3. Model Training and Verifying. The engine valve fault identification experiment was stratified into two parts, namely, building the fault identification model by model

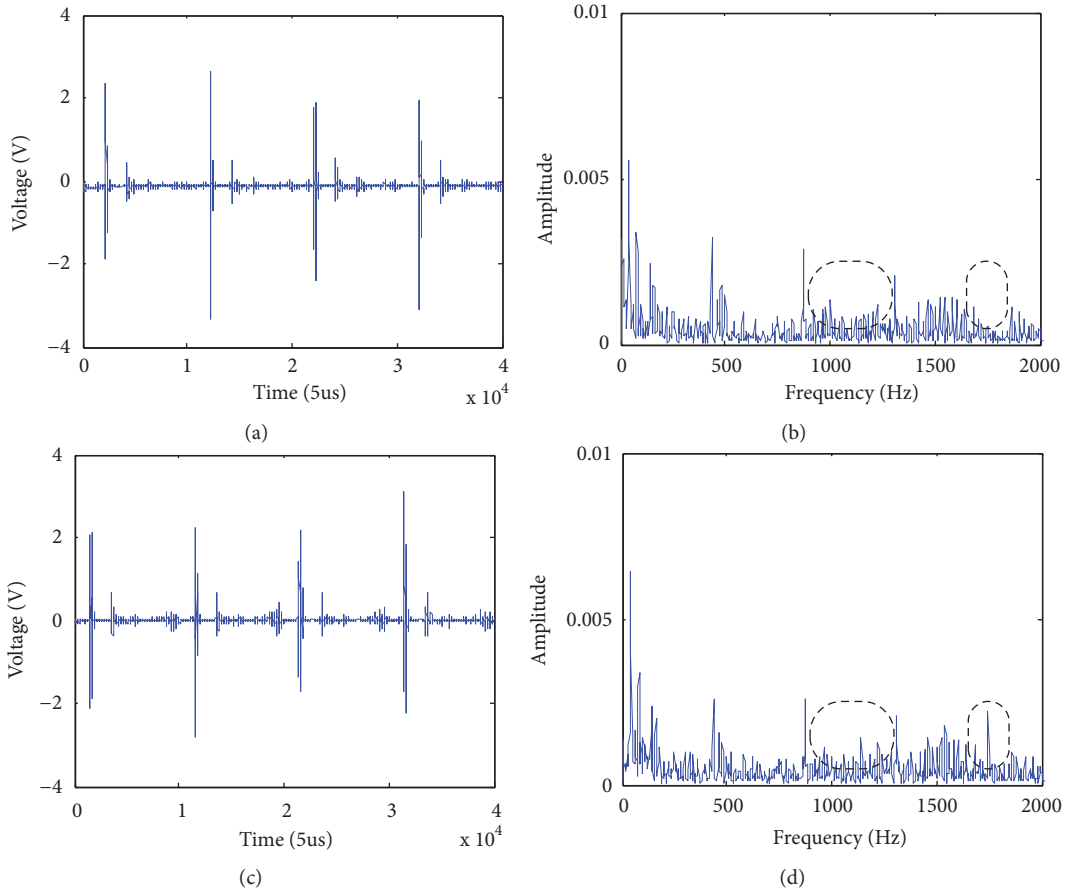

Figure 7: Comparison of time domain and frequency domain characteristics. (a) Time domain diagram of normal state signal, (b) frequency diagram of normal state signal, (c) time domain diagram of abnormal state signal, and (d) frequency diagram of abnormal state signal.

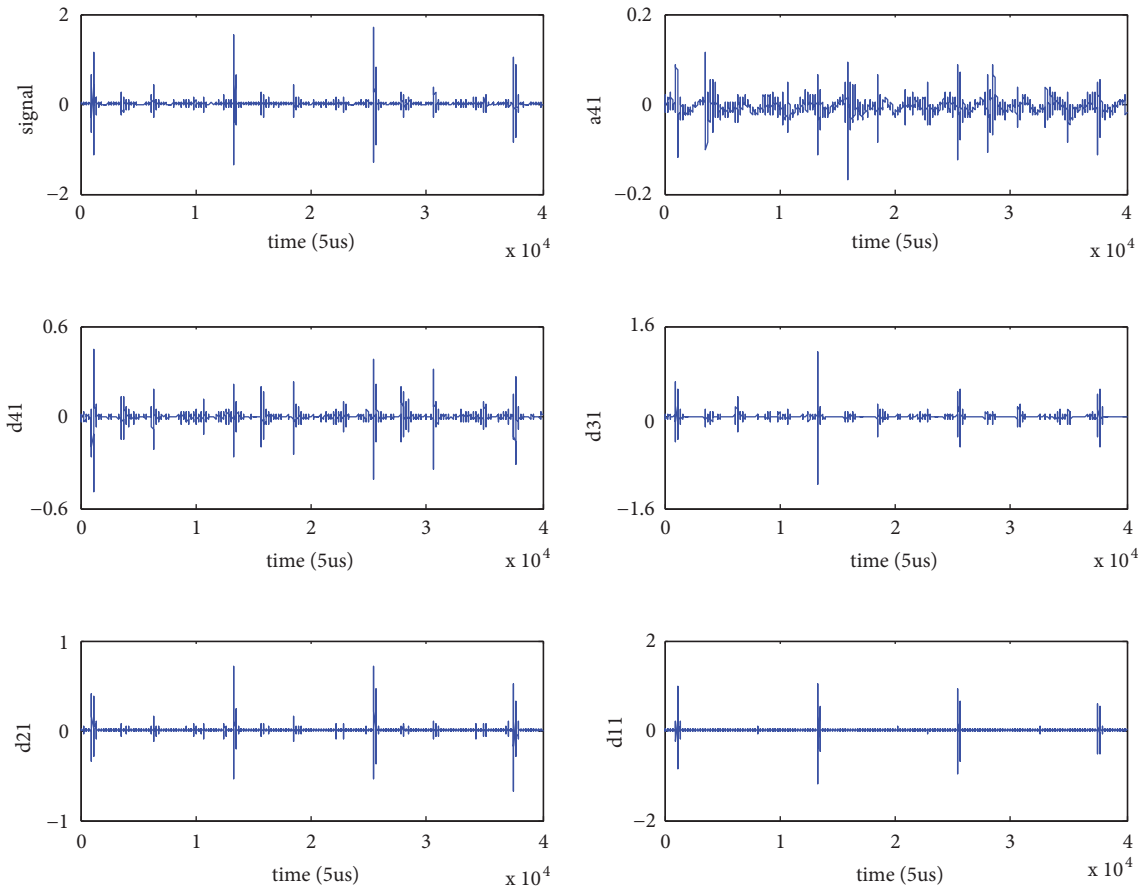

Figure 8: The decomposed vibration signals of fault type I.

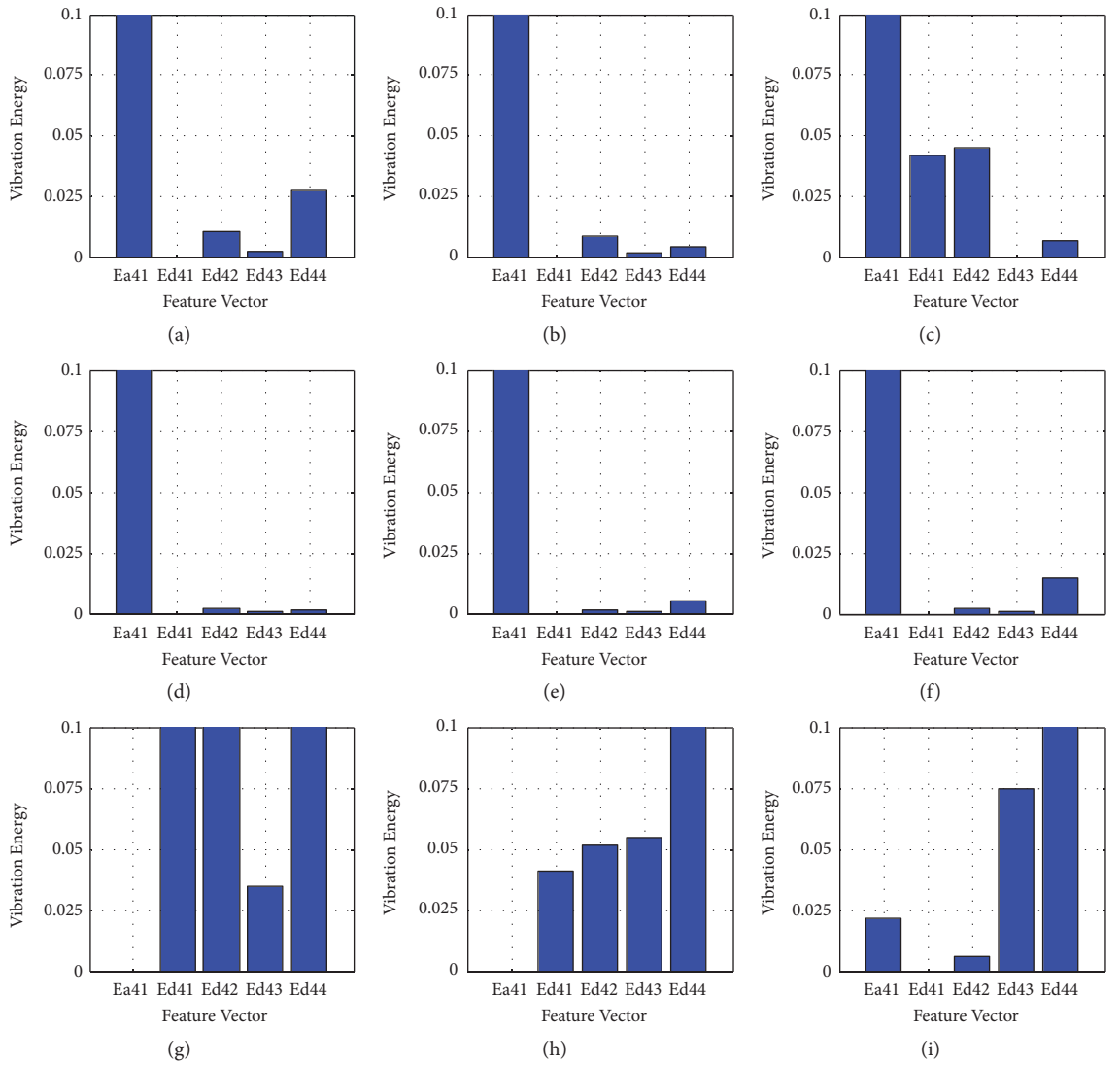

Figure 9: The characteristics of different fault feature vector: (a) fault type I, (b) fault type II, (c) fault type III, (d) fault type IV, (e) fault type V, (f) fault type VI, (g) fault type VII, (h) fault type VIII, and (i) fault type IX.

training and verifying the constructed model by model testing.

For model training, the experiments were performed 3 times on ZH195 diesel engine by keeping the engine speed from 800 rpm to 1200 rpm at 200 rpm steps under no-load condition. Thus, 9 groups of vibration signals were obtained, and the fault features were extracted. Subsequently, the engine state shifted from fault II to fault IX, and the same experiments were performed. 81 groups of vibration signals were detected, and the fault features were extracted. Finally, the fault detection model based on multiclass υ-SVC was trained. In this study, hyperparameter γ was set as 4, and hyperparameter υ was set as 32 using the cross validation. The training result is shown in Figure 10. It is found that the multiclassification υ-SVC method identified different fault type accurately.

When the model was built, further experiments were performed from fault I to fault IX, and the experiment count was set as 162. Thus, 162 groups of vibration signals and their relevant fault feature were extracted to verify the correctness of the model. The result is shown in Figure 11, showing that the average accuracy of fault identification reached 96.3%. The result here reveals that the proposed fault identification method can be effectively used for diagnosing the engine fault.

The fault identification performance of the built model based on υ-SVC was compared with the results of SOM (Self-Organization feature Map) neural network. The SOM neural network refers to a self-organizing, self-learning network consisting of a fully connected array of neurons [25]. It is preferred for fault classification for its high accuracy even with small samples. The number of competitive layer neurons

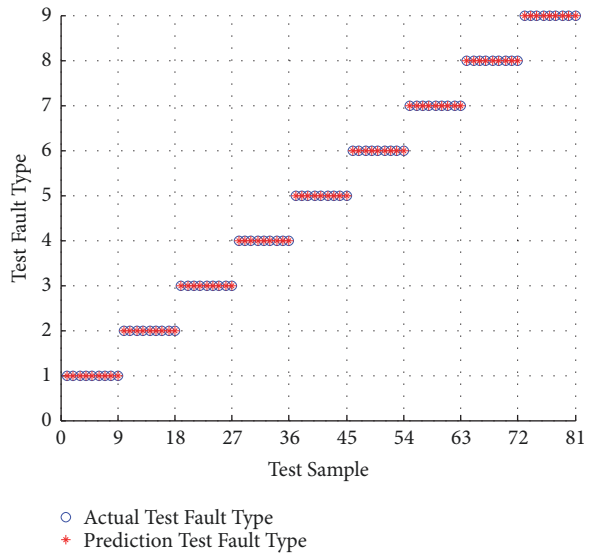

Figure 10: The training results of the fault type identification.

Table 4: Feature vector based on Wavelet decomposition and reconstruction.

Operating state	No.	vibration energy feature vector				
		E_{a41}	E_{d41}	E_{d31}	E_{d21}	E_{d11}
Fault type I	1	29171.56	125.61	419.31	190.47	916.02
	2	28467.95	314.92	536.79	310.96	615.85
	3	29162.03	657.91	1198.32	743.29	1532.70
Fault type II	1	34728.80	157.96	446.43	203.43	305.95
	2	37501.9	442.93	787.90	364.83	757.68
	3	41248.90	604.38	1035.80	783.93	1459.29
Fault type III	1	51984.62	2601.75	2774.43	440.82	774.74
	2	66161.88	3606.90	4286.53	2143.04	3459.64
	3	55689.37	10129.43	4527.10	3965.93	7854.19
Fault type IV (Normal)	1	86067.38	133.12	327.000	195.39	288.40
	2	84843.81	267.18	464.92	343.86	844.38
	3	84297.88	542.58	1182.75	710.60	2152.55
Fault type V	1	70662.03	155.80	281.01	201.87	520.20
	2	70043.63	302.41	671.87	496.92	1467.39
	3	70177.78	611.64	1671.62	703.10	1696.39
Fault type VI	1	66528.25	338.03	491.06	398.17	1325.69
	2	66243.20	673.17	1596.44	839.55	1802.04
	3	67345.94	956.43	1467.58	1159.19	2497.36
Fault type VII	1	187.27	824.61	876.71	328.32	4278.87
	2	176.31	387.19	104.38	477.13	4155.92
	3	208.67	741.50	100.80	341.36	3565.39
Fault type VIII	1	115.19	304.61	353.27	367.06	4727.75
	2	173.00	608.37	891.72	459.13	3843.63
	3	136.02	962.09	780.94	932.79	4177.78
Fault type IX	1	275.42	163.24	194.65	550.57	5338.03
	2	200.03	109.90	118.59	400.76	4896.44
	3	231.09	130.74	178.99	557.56	6101.87

Table 5: Identification results.

Method	Identification accuracy				
	FaultType	Number of samples	Correct identification number	Accuracy (%)	Average accuracy (%)
υ-SVC	I	18	18	100.0	96.3
	II	18	18	100.0	
	III	18	17	94.4	
	IV	18	18	100.0	
	V	18	17	94.4	
	VI	18	18	100.0	
	VII	18	17	94.4	
	VIII	18	17	94.4	
	IX	18	16	88.9	
SOM neural network	I	18	17	94.4	88.9
	II	18	17	94.4	
	III	18	16	88.9	
	IV	18	17	94.4	
	V	18	17	94.4	
	VI	18	16	88.9	
	VII	18	16	88.9	
	VIII	18	16	88.9	
	IX	18	15	83.3	

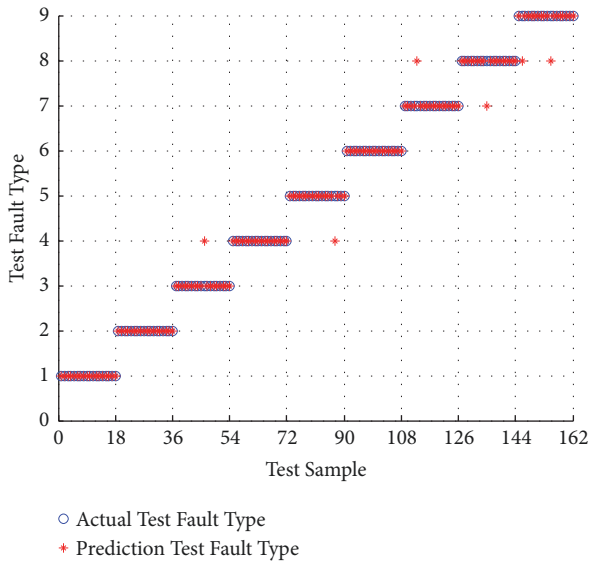

Figure 11: The verifying results of the fault type identification.

was set as 36, and the number of training steps was set as 500. The identification results are listed in Table 5, showing that the fault model based on υ-SVC achieved higher fault identification rates.

4. Conclusions

In the present study, a novel ICE fault identification method combining FBG vibration sensor and SVM was proposed. The experimental tests on the valve fault and fuel injection advance angle fault were performed and presented to verify the efficacy of the newly proposed approach. The experimental case studies reveal that the proposed method exhibit excellent fault detection performance for ICE fault identification. Compared with SOM neural network-based method, the proposed method can achieve higher fault identification rates. Thus, this study provided a practical and effective device for ICE fault identification in future research.

Data Availability

The data used to support the findings of this study are available from the corresponding author upon request.

Conflicts of Interest

The authors declare that they have no conflicts of interest.

Acknowledgments

This research was supported by the Natural Science Foundation of Shandong Province (grant number ZR2017PEE023); the Fundamental Research Funds of Shandong University (grant number 2018JCG06); the Key Research and Development Plan of Shandong Province (2017CXGC0610); the National Natural Science Foundation of China (grant number 61873333); and the Young Scholars Program of Shandong University (grant number 2016WLJH30).

References

[1] V. T. Tran, F. Althobiani, and A. Ball, "An approach to fault diagnosis of reciprocating compressor valves using Teager–Kaiser energy operator and deep belief networks," *Expert Systems with Applications*, vol. 41, no. 9, pp. 4113–4122, 2014.

[2] C. Wang, Y. Zhang, and Z. Zhong, "Fault diagnosis for diesel valve trains based on time-frequency images," *Mechanical Systems and Signal Processing*, vol. 22, no. 8, pp. 1981–1993, 2008.

[3] Y. Zhang, L. Duan, and M. Duan, "A new feature extraction approach using improved symbolic aggregate approximation for machinery intelligent diagnosis," *Measurement*, vol. 133, pp. 468–478, 2019.

[4] Z. Feng, H. Ma, and M. J. Zuo, "Vibration signal models for fault diagnosis of planet bearings," *Journal of Sound and Vibration*, vol. 370, pp. 372–393, 2016.

[5] Z. Zhou, Q. Liu, Q. Ai, and C. Xu, "Intelligent monitoring and diagnosis for modern mechanical equipment based on the integration of embedded technology and FBGS technology," *Measurement*, vol. 44, no. 9, pp. 1499–1511, 2011.

[6] J. Salo and I. Korhonen, "Calculated estimate of FBG sensor's suitability for beam vibration and strain measuring," *Measurement*, vol. 47, no. 1, pp. 178–183, 2014.

[7] B. de Pauw, A. Lamberti, J. Ertveldt et al., "Vibration monitoring using fiber optic sensors in a lead-bismuth eutectic cooled nuclear fuel assembly," *Sensors*, vol. 16, no. 4, Article ID s16040571, 2016.

[8] K. Oman, B. Van Hoe, K. Aly et al., "Instrumentation of integrally stiffened composite panel with fiber Bragg grating sensors for vibration measurements," *Smart Materials and Structures*, vol. 24, no. 8, Article ID 085031, 2015.

[9] A. Lamberti, B. De Pauw, and S. Vanlanduit, "Development of an optical fiber sensor interrogation system for vibration analysis," *Journal of Sensors*, vol. 2016, Article ID 5204581, 8 pages, 2016.

[10] Z. Liu, Y. Liu, D. Zhang, B. Cai, and C. Zheng, "Fault diagnosis for a solar assisted heat pump system under incomplete data and expert knowledge," *Energy*, vol. 87, pp. 41–48, 2015.

[11] D. Ma, Y. Liang, X. Zhao, R. Guan, and X. Shi, "Multi-BP expert system for fault diagnosis of powersystem," *Engineering Applications of Artificial Intelligence*, vol. 26, no. 3, pp. 937–944, 2013.

[12] Y. Zhi-Ling, W. Bin, D. Xing-Hui, and L. Hao, "Expert system of fault diagnosis for gear box in wind turbine," *Systems Engineering Procedia*, vol. 4, pp. 189–195, 2012.

[13] S. J. S. Hakim, H. Abdul Razak, and S. A. Ravanfar, "Fault diagnosis on beam-like structures from modal parameters using artificial neural networks," *Measurement*, vol. 76, pp. 45–61, 2015.

[14] W. Chine, A. Mellit, V. Lughi, A. Malek, G. Sulligoi, and A. Massi Pavan, "A novel fault diagnosis technique for photovoltaic systems based on artificial neural networks," *Journal of Renewable Energy*, vol. 90, pp. 501–512, 2016.

[15] L. S. Dhamande and M. B. Chaudhari, "Detection of combined gear-bearing fault in single stage spur gear box using artificial neural network," in *Proceedings of the 12th International Conference on Vibration Problems, ICOVP 2015*, pp. 759–766, India, December 2015.

[16] A. Torabi Jahromi, M. J. Er, X. Li, and B. S. Lim, "Sequential fuzzy clustering based dynamic fuzzy neural network for fault diagnosis and prognosis," *Neurocomputing*, vol. 196, pp. 31–41, 2016.

[17] H. Merabet, T. Bahi, and N. Halem, "Condition monitoring and fault detection in wind turbine based on DFIG by the fuzzy logic," in *Proceedings of the International Conference on Technologies and Materials for Renewable Energy, Environment and Sustainability, TMREES 2015*, pp. 518–528, Lebanon, April 2015.

[18] J. Zheng, J. Cheng, Y. Yang, and S. Luo, "A rolling bearing fault diagnosis method based on multi-scale fuzzy entropy and variable predictive model-based class discrimination," *Mechanism and Machine Theory*, vol. 78, pp. 187–200, 2014.

[19] V. N. Vapnik, *The Nature of Statistical Learning Theory*, Springer, New York, NY, USA, 1995.

[20] Z. Liu, H. Cao, X. Chen, Z. He, and Z. Shen, "Multi-fault classification based on wavelet SVM with PSO algorithm to analyze vibration signals from rolling element bearings," *Neurocomputing*, vol. 99, pp. 399–410, 2013.

[21] F. Chen, B. Tang, and R. Chen, "A novel fault diagnosis model for gearbox based on wavelet support vector machine with immune genetic algorithm," *Measurement*, vol. 46, no. 1, pp. 220–232, 2013.

[22] V. Muralidharan, V. Sugumaran, and V. Indira, "Fault diagnosis of monoblock centrifugal pump using SVM," *Engineering Science and Technology, an International Journal*, vol. 17, no. 3, pp. 152–157, 2014.

[23] B. Gu and V. S. Sheng, "A robust regularization path algorithm for v-Support Vector Classification," *IEEE Transactions on Neural Networks Learning Systems*, pp. 1–8, 2016.

[24] J. Lee, H. Kim, N.-R. Kim, and J.-H. Lee, "An approach for multi-label classification by directed acyclic graph with label correlation maximization," *Information Sciences*, vol. 351, pp. 101–114, 2016.

[25] B. Merainani, C. Rahmoune, D. Benazzouz, and B. Ould-Bouamama, "A novel gearbox fault feature extraction and classification using Hilbert empirical wavelet transform, singular value decomposition, and SOM neural network," *Journal of Vibration and Control*, vol. 24, no. 12, pp. 2512–2531, 2018.